J Mol Model (2013) 19:4503–4510
DOI 10.1007/s00894-013-1960-3

ORIGINAL PAPER

Direct dynamics simulations of the hydrogen abstraction reaction $Cl+CF_3CF_2CH_2OH$

Ang-yang Yu · Hong-xing Zhang

Received: 9 June 2013 / Accepted: 24 July 2013 / Published online: 14 August 2013

Abstract The mechanism and kinetics of 2,2,3,3,3-pentafluoropropanol ($CF_3CF_2CH_2OH$) reaction with Chlorine atom (Cl) is investigated in this work. Two hydrogen abstraction channels of the title reaction are identified. The geometries of all the stationary points in the potential energy surface are obtained at the BHandHLYP/6-311G** level, and the energies of the selected points along the minimum energy path (MEP) are improved by the CCSD(T) method. A dual-level direct dynamics method is employed to study the kinetic nature of the hydrogen-abstraction reaction channels. The calculated rate coefficients show that the hydrogen abstraction from the CH_2 group is the primary channel. The calculated total rate coefficients are in best agreement with the experimental values. The four-parameter rate coefficients expression of the title reaction between the temperatures 200 K and 1000 K is provided.

Keywords $CF_3CF_2CH_2OH$ · Direct dynamics · Hydrogen abstraction · Rate coefficients · Variational transition-state theory

Introduction

Fully halogenated chlorofluorocarbons (CFCs) are the sources of the depletion of the stratospheric ozone layer and global warming. According to the Montreal protocol, hydrofluorocarbons (HFCs) have been regarded as the new generation of CFC substitutes, since they do not contain chlorine or bromine atoms and they are expected to be more reactive in the troposphere. Although $-CF_3$ groups of HFCs do not contribute to the stratospheric ozone depletion [1], they may potentially enhance the global warming effect [2]. Recently, hydrofluoroethers (HFEs) and hydrogenated fluorinatedalcohols (HFAs) have been considered as alternatives for HFCs in a variety of industrial applications including paints, coatings, polymers and so on [3]. Therefore, it is essential to extend the knowledge about their atmospheric reactions and environmental impact of these kind of compounds.

Tropospheric degradation of HFAs will mainly happen though the reaction with hydroxyl (OH) radicals in the daytime. However, the oxidation by chlorine atoms has gained great importance in recent years because they could exert some influence at the boundary layer, particularly in marine and coastal environments, and in the Arctic troposphere during springtime [4]. The main cause of tropospheric chlorine atoms is the photolysis of chlorine-containing molecules generated by heterogeneous reactions of sea salt aerosols [5, 6]. However, it has also been proposed that Cl atoms, produced in the photolysis of Cl_2 emitted from industrial processes, may enhance hydrocarbon oxidation rates and ozone production in urban environments [7, 8].

2,2,3,3,3-pentafluoropropanol, $CF_3CF_2CH_2OH$, is a characteristic HFA which can replace CFCs as cleaning agents [3]. Its reaction with OH radicals has been studied experimentally [9–12] and theoretically [13]. Nevertheless, there are only three experimental kinetic studies on the $CF_3CF_2CH_2OH+Cl$ reaction [11, 14]. Hurley et al. [11] reported a relative rate coefficient measurement at room temperature, while Papadimitriou et al. [14] employed an absolute technique to determine the temperature dependence of the rate coefficient at very low pressures. Recently, a pulsed laser photolysis-resonance fluorescence (PLP-RF) technique has been used to determine the rate coefficients for the $CF_3CF_2CH_2OH+Cl$ reaction within the atmospheric pressure range of 50–200 Torr and in the temperature range of 268–377 K. The first step of the $CF_3CF_2CH_2OH+Cl$ reaction was also theoretically

A.-y. Yu (✉) · H.-x. Zhang
State Key Laboratory of Theoretical and Computational Chemistry, Institute of Theoretical Chemistry, Jilin University, Changchun 130023, China
e-mail: wisdomyay@163.com

investigated by Garzon et al. [15]. In spite of these advances mentioned above, theoretical work of the mechanism of this reaction is still limited. Therefore, it is necessary to carry out a more detailed kinetics study of the title reaction which thus forms the motivation of this theoretical work. Our aims are to investigate the possible reaction mechanisms and feasible channels, to obtain the most accurate theoretical rate coefficients, to explore to what extent these theoretical predictions could be compared with available experimental results and settle the disagreement between previous theoretical and experimental results [15] in the temperature range 268–377 K.

Computational details and theory

Electronic structure calculations

It has been shown that Beck's half and-half (BH&H) [16] nonlocal exchange and the Lee-Yang-Parr [17] correlation functional method provides a good alternative for a wide variety of applications, in particular, for direct dynamics simulations [18, 19]. Therefore, the geometries and frequencies of all stationary points including the reactants, products, and the transition states are optimized at the Beck's half and-half (BH&H) nonlocal exchange and the Lee-Yang-Parr with the 6-311G** basis set in the present study. At the same level, the minimum energy path (MEP) is obtained by intrinsic reaction coordinate theory (IRC) to confirm that the transition state really connects the minima along the path. Along the reaction path, the reaction coordinate s is defined as the signed distance from the saddle point, with s>0 standing for the product side and s<0 referring to the product side. At 20 selected points along the MEP, the force constant matrices as well as the harmonic vibrational frequencies were calculated at the same level. To obtain more accurate energies and barrier height, the single point energies (SPE) of all the stationary points and selected points along the minimum energy path (MEP) were refined by the coupled-cluster [20] (CC) theory of triple excitations CCSD(T) method [21]. What is more, the reactant and product complexes are also found at the entrance and exit of each channel for the title reaction. All of the electronic structure calculations were performed with the Gaussian 09 program [22].

Rate coefficient calculations

A dual-level(X//Y) direct dynamics method [23–25] is employed in the present work to investigate the title reaction. In order to calculate the rate coefficients of the title reaction, we use the variational transition-state theory (VTST). Canonical variational transition-state theory [26] (CVT) with the small-curvature tunneling (SCT) approximation [27, 28] is chosen as the level of VTST. The CVT rate coefficient for temperature T is expressed as:

$$k^{CVT}(T,s) = \min k^{GT}(T,s) \tag{1}$$

and

$$k^{GT}(T,s) = \kappa(T)\frac{\sigma k_B T}{h}\frac{Q^{GT}(T,S)}{\Phi^R(T)}e^{-V_{MEP}(s)\Big/k_B T} \tag{2}$$

where $k^{GT}(T, s)$ is the rate coefficient in generalized transition state theory at the dividing surface s, with σ being the reaction symmetry number accounting for the possibility of more than one symmetry related reaction path, k_B is the Boltzmann's coefficient, h is the Planck's coefficient, $\kappa(T)$ is the transmission coefficient accounting for the quantum mechanical tunneling effects, $Q^{GT}(T, s)$ and $\Phi^R(T)$ are the total partition functions (per unit volume) of the transition state and reactants, respectively. The separable translational, vibrational, rotational, and electronic motion assumption is used to evaluate the partition functions. In calculating electronic partition function, we included the $^3P_{3/2}$ and $^2P_{1/2}$ electronic states of Cl atom, with an 881 cm^{-1} splitting due to the spin-orbit coupling. The rotational and translation partition functions are calculated classically. Most of the vibrational modes are treated as quantum mechanical separable harmonic oscillators, while the two low-frequency modes which correspond to hindered rotations are treated as hindered rotors. The hindered rotor approximation of Truhlar and Chuang [29, 30] is used for calculating the partition function of them. The total rate coefficients are obtained from the sum of the individual rate coefficients. In addition, the title reaction involves hydrogen transfer processes and tunneling is expected to be noticeable for such steps, therefore, the SCT tunneling method [31–33] is employed to calculate the transmission coefficient in the evaluation of the CVT rate coefficients. In summary, the canonical variational transition-state theory (CVT) with the small-curvature tunneling (SCT) corrections is applied to evaluate the theoretical rate coefficients. All the dynamical calculations are performed using the general polyatomic rate coefficients code Polyrate9.6 program [34]. In the end, the comparison between theoretical and experimental rate coefficients is discussed.

Results and discussion

Stationary points

In the recent work performed by Garzon et al. [15], the transition states (TSs), the molecular complexes (MCs) and

minimum energy path (MEP) were calculated at the MP2/6-311G** level. However, the choice of the MP2 approach for the calculations of the minimal energy path is questionable. MP2 is known to be susceptible to significant spin contamination, especially for vibrational frequency calculations, which are used in computation of rate coefficients. In the current work, the geometry of the reactant 2,2,3,3,3-pentafluoropropanol is calculated at the BHandHLYP/6-311G** level. Quantum chemical analysis of the energies of the anti and gauche conformers of $CF_3CF_2CH_2OH$ has also been made. The results show that the gauche conformation of the reactant $CF_3CF_2CH_2OH$ is the most stable conformation which is consistent with previous conformation analysis [35]. Hence, the subsequent transition states are calculated from the most stable gauche conformer of $CF_3CF_2CH_2OH$. For the reactant $CF_3CF_2CH_2OH$, two hydrogen atoms in the CH_2 group are equivalent, thus one hydrogen abstraction channel from the CH_2 group is found (channel R1). Moreover, the Cl

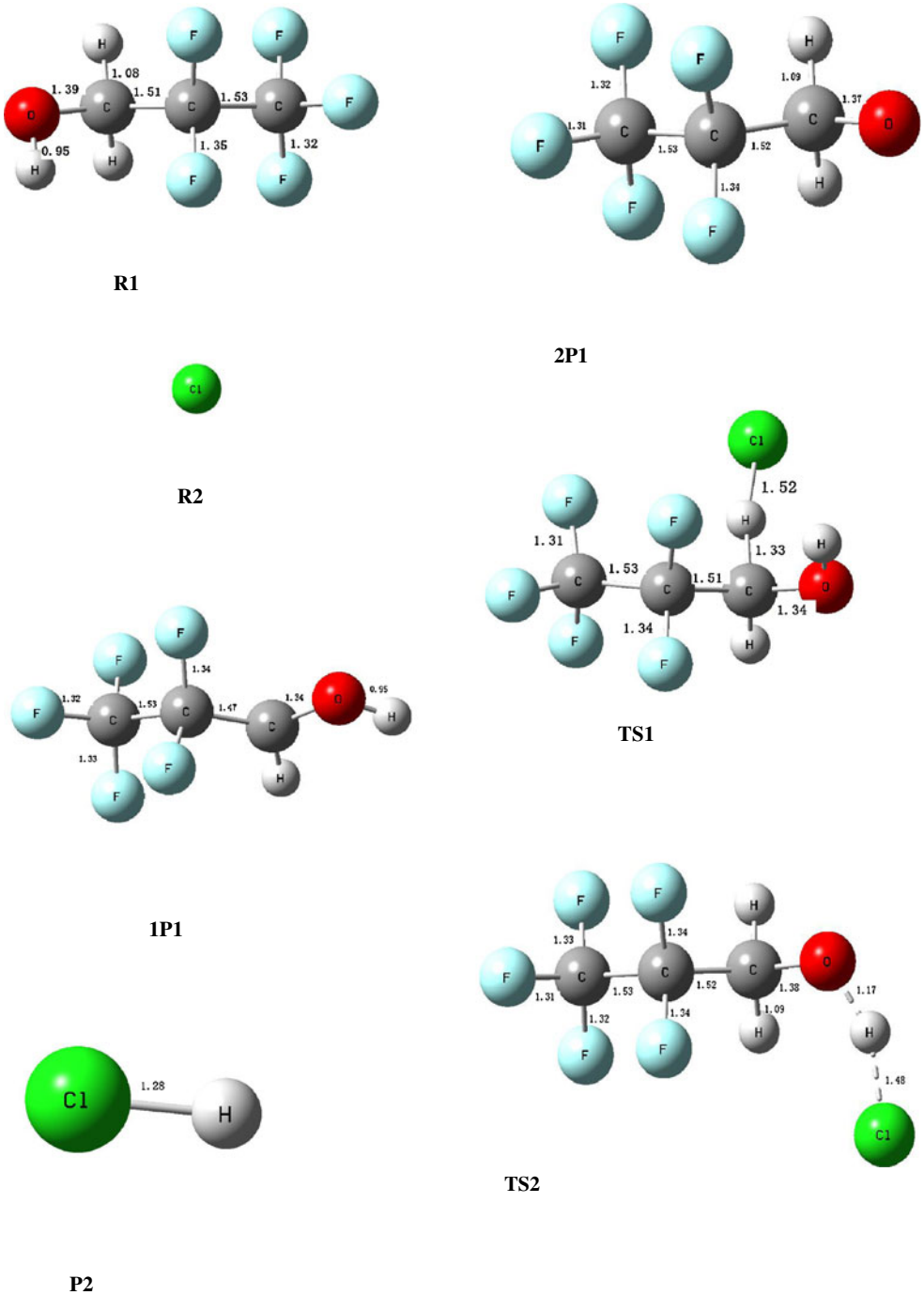

Fig. 1 Optimized geometries of reactants, products and the transition states at the BHandHLYP/6-311G** level. Bond length is in angstrom

atom can also attack the OH group in the reactant $CF_3CF_2CH_2OH$ and produce HCl and $CF_3CF_2CH_2O$ (channel R2). Thus, two hydrogen abstraction channels are feasible for the $Cl+CF_3CF_2CH_2OH$ reaction as listed below:

$$CF_3CF_2CH_2OH+Cl\rightarrow CF_3CF_2CHOH+HCl\ R1$$
$$CF_3CF_2CH_2OH+Cl\rightarrow CF_3CF_2CH_2O+HCl\ R2$$

The reactant and product complexes of the two hydrogen abstraction channels are located at the entrance and exit of the reactions, indicating that the two hydrogen abstraction channels may proceed via an indirect mechanism. Table 1 lists the structural parameters of all of the reactants, products and reaction complexes for the two reaction channels R1 and R2, which are calculated by the BHandHLYP/6-311G** level of theory. For the convenience of the readers, Fig. 1 presents the optimized geometric parameters of the reactants (Cl atom and $CF_3CF_2CH_2OH$), the products (CF_3CF_2CHOH, $CF_3CF_2CH_2O$, and HCl) and the transition states (TS1 and TS2) calculated at the BHandHLYP level with the 6-311G** basis set. For the transition-state structure TS1 in the reaction channel R1, the length of the breaking C-H bond increases by 22%, with respect to the corresponding equilibrium bond length of the reactant ($CF_3CF_2CH_2OH$) at the BHandHLYP/6-311G** level of theory. Meanwhile, the length of the forming Cl-H bond in the transition state TS1, which will form the HCl molecule, is 18.8% longer than the equilibrium bond length of the HCl molecule. The elongation of the forming Cl-H bond is less than that of the breaking O-H bond, which indicates that the two transition states are all product-like, and the reaction may proceed via late transition state for the reaction channel R1. The case is similar for the transition state TS2. In the transition state structure TS2, the breaking bond O-H is elongated by 23.3% compared to the O-H equilibrium bond length of $CF_3CF_2CH_2OH$, and the forming Cl-H bond is 16.0% longer than the regular bond length of the isolated HCl molecule which indicates that the geometric feature of TS2 is characteristic of the late transition state.

Table 2 lists the harmonic vibrational frequencies of all of the stationary points which include the reactants, products, transition states and complexes calculated at the BHandHLYP/6-311G** level. As can be seen from the table, all of the local minima including reactants, products and complexes correspond to all real frequencies, and the transition states are confirmed by normal-mode analysis to have only one imaginary frequency whose eigenvector corresponds to the direction of the

Table 1 Calculated frequencies (in cm^{-1}) and zero-point energy (in kcal mol^{-1}) of the stationary points at the BHandHLYP/6-311G** Level

Species	Frequencies	ZPE
R1($CF_3CF_2CH_2OH$)	62,103,168,229,288,339,353,385,410,468,549,613,614,762,834,992, 1,086,1,168,1,207,1,285,1,289,1,326,1,338,1,435,1,471,1,506,1,554,3,124, 3,219,3,992	46.0
P1a(CF_3CF_2CHOH)	64,71,169,223,281,299,358,375,391,448,550,581,616,644,762, 842,1,092,1,153,1,220,1,285,1,301,1,338,1,347,1,453,1,570,3,291,4,016	36.8
P2a (CF_3CF_2CHO)	57,95,174,228,284,348,352,387,461,547,615,615,742,823,1,060, 1,069,1,159,1,270,1,293,1,327,1,341,1,379,1,467,1,502,1,575,3,105,3,169	37.8
HCl ($C_{\infty v}$)	3,046	4.4
TS1	1179i,21,65,86,159,173,228,275,310,357,388,413,460,543,577, 621,625,770,845,956,1,082,1,118,1,206,1,227,1,262,1,281,1,308,1,334, 1,375,1,455,1,507,3,250,3,936	41.8
TS2	2006i,32,46,66,141,176,226,281,348,356,384,403,457,549,613,614, 758,796,848,960,1,057,1,098,1,182,1,219,1,285,1,291,1,340,1,359,1,442, 1,472,1,489,3,110,3,190	40.9
CR1	13,36,51,67,113,167,229,287,337,353,385,401,467,548,613,614,763, 834,989,1,084,1,168,1,201,1,285,1,289,1,327,1,341,1,439,1,470,1,504,1,552, 3,127,3,216,3,986	46.1
CP1	13,26,56,64,79,177,188,208,227,284,300,360,379,392,450,544,570, 614,638,759,840,1,088,1,156,1,224,1,269,1,299,1,340,1,350,1,449,1,573, 3,025,3,296,4,006	41.8
CR2	29,46,66,101,115,188,229,302,354,361,394,456,503,551,615,615,763, 837,992,1,082,1,158,1,203,1,286,1,292,1,322,1,339,1,429,1,462,1,505,1,555, 3,149,3,235,3,968	46.5
CP2	15,32,56,80,81,176,227,239,278,318,352,355,389,461,548,615,615, 743,823,1,066,1,068,1,151,1,266,1,295,1,330,1,346,1,376,1,465,1,523,1,573, 3,002,3,115,3,190	43.1

reaction. The absolute values of imaginary frequencies for TS1 and TS2 are 1179 and 2006 cm^{-1}, respectively. Since these two transition states possess large absolute values of the imaginary frequencies, this means that the quantum tunneling transmission coefficient should be large and the quantum tunneling effects should be important in the evaluation of the rate coefficients.

The reaction enthalpies ΔH^0_{298K} of the two reaction channels calculated at the CCSD(T)//BHandHLYP/6-311G** level of theory for the two reaction channels are listed in Table 3. The potential barriers (ΔE in kcal mol^{-1}) considering zero point energy (ZPE) correction are also included. As shown in the table, the reaction channel R1 is endoergic with the $\Delta H^0_{298\ K}$ value of 3.33 kcal mol^{-1} while the reaction channel R1 is exothermic for channel R2 with the $\Delta H^0_{298\ K}$ value of 7.18 kcal mol^{-1}.

Table 3 Calculated CVT/SCT rate coefficients (in $cm^3molecule^{-1}s^{-1}$) for the title reaction at the CCSD(T)//BHandHLYP/6-311G** level

T(K)	k_1	k_2	k	Exp
200	8.94E–14	4.51E–25	8.94E–14	
230	1.36E–13	6.31E–25	1.36E–13	
268	2.21E–13	9.52E–25	2.21E–13	6.37E–13
272	2.33E–13	9.94E–25	2.33E–13	6.41E–13
285	2.73E–13	1.14E–24	2.73E–13	6.66E–13
298	3.19E–13	1.31E–24	3.19E–13	7.23E–13
316	3.93E–13	1.58E–24	3.93E–13	7.53E–13
337	4.98E–13	1.98E–24	4.98E–13	8.02E–13
359	6.31E–13	2.50E–24	6.31E–13	8.69E–13
377	7.61E–13	3.04E–24	7.61E–13	9.11E–13
450	1.51E–12	6.76E–24	1.51E–12	
600	4.60E–12	3.46E–23	4.60E–12	

Reaction path properties

As mentioned in the previous section, the geometries of points along the MEP were optimized by the BHandHLYP/6-311G** level of theory. Starting from the saddle-point geometries, the minimum energy path (MEP) which goes downhill to both the asymptotic reactants and the products in the mass-weighted internal coordinates is obtained by the intrinsic reaction coordinate (IRC) theory. Along this minimum energy path (MEP), the reaction coordinate, s, is defined as the signed distance from the saddle point, with s>0 referring to the product side. The Hessian matrix was evaluated at the selected points along the reaction path using the same level of theory. However, in a recent work of the title reaction [15], the minimum energy path was calculated at QCISD(T) level corrected with thermal corrections estimated at MP2(full)/6-311G**. The method of QCISD(T) for energy calculations is far from a state-of-the-art level of theory where much better calculations can be easily used for this reaction. It has been agreed coupled cluster method is always preferred over QCI and the computational cost is identical (terms neglected in QCI are not time-consuming). Hence, the potential energy profiles are refined at the CCSD(T) level of theory in the current work.

A schematic potential energy surface of the title reaction obtained at the CCSD(T)//BHandHLYP level considering the zero point energy (ZPE) correction is plotted in Fig. 2. The energy of the reactant is set to be zero as a reference. As shown in Fig. 2, the reaction of the Cl atom with $CF_3CF_2CH_2OH$ may start from the attractive wells in the entrance valleys of the potential energy surfaces, forming the complexes CR1 or CR2. The stabilization energies are 1.53 and 4.46 kcal mol^{-1} for CR1 and CR2, respectively. Then, each reactant complex undergoes a hydrogen transfer process to form product complexes CP1 and CP2, which lie 2.27 and 3.21 kcal mol^{-1} below the products' energies of the corresponding channels, respectively. With respect to the barrier heights of channels R1 and R2, the energies are 5.83 kcal mol^{-1} (TS1) and 15.83 kcal mol^{-1} (TS2), respectively. The potential barrier height for channel R1, which is the hydrogen abstraction from the CH_2 group of

Table 2 Parameters (in kcal mol^{-1}) at the CCSD(T)//BHandHLYP/6-311G** level for the two reaction channels

Channels	ΔE^a	$\Delta H^0_{298K}{}^b$
$CF_3CF_2CH_2OH+Cl \rightarrow CF_3CF_2CHOH+HCl$	5.83	−3.33
$CF_3CF_2CH_2OH+Cl \rightarrow CF_3CF_2CH_2O+HCl$	15.83	7.18

[a] Potential barriers (in kcal mol^{-1}) considering ZPE correction

[b] Reaction relative enthalpies (in kcal mol^{-1}) calculated

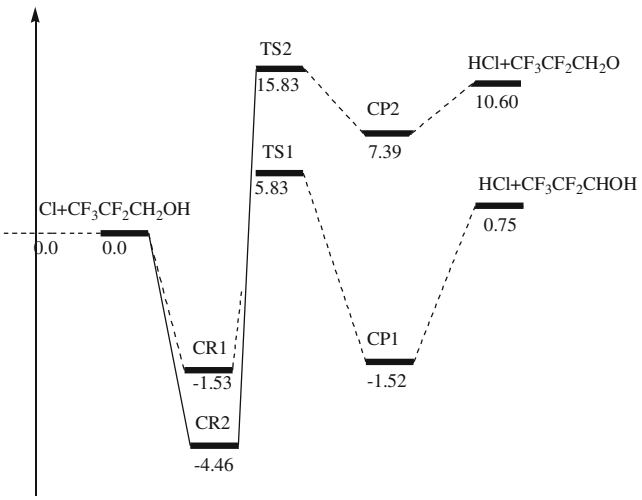

Fig. 2 Schematic potential energy surface for the reaction $CF_3CF_2CH_2OH+Cl$

the reactant $CF_3CF_2CH_2OH$ (kcal mol^{-1}) is the lowest one. Correspondingly, the barrier height of the reaction channel R2 is much larger than the counterpart of channel R1. Therefore, channel R1 may be the major reaction pathway and the other channel R2 would be less favorable. Based on the analysis above, we could anticipate that the rate coefficients for the hydrogen abstraction channel R2 could be ignored and we will further confirm this prediction in the following section.

The classical potential energy curves (V_{MEP}), the zero point energy (ZPE) curves and vibrationally adiabatic ground-state potential energy curves (V_a^G) for the two reaction channels as functions of the reaction coordinate s ($(amu)^{1/2}$bohr) are presented in Fig. 3 at the BHandHLYP/6-311G** level for the title reaction, where $V_a^G(s)=V_{MEP}(s)+ZPE$. It can be seen from the zero point energy curve that the ZPE is practically constant as s varies, with only a gentle drop near the saddle point. The $V_{MEP}(s)$ and the $V_a^G(s)$ energy curves are similar in shape. It could be seen from these two figures that the maxima of the $V_{MEP}(s)$ and the $V_a^G(s)$ energy curves are located at the same position, implying that the variational effect will be small or almost negligible for the kinetic studies. In addition, all the reaction channels are the hydrogen atom transfer reactions. Therefore, the tunneling effect should play a significant role in the lower-temperature region for each channel. These predictions mentioned above will be further testified in the subsequent rate coefficient calculations.

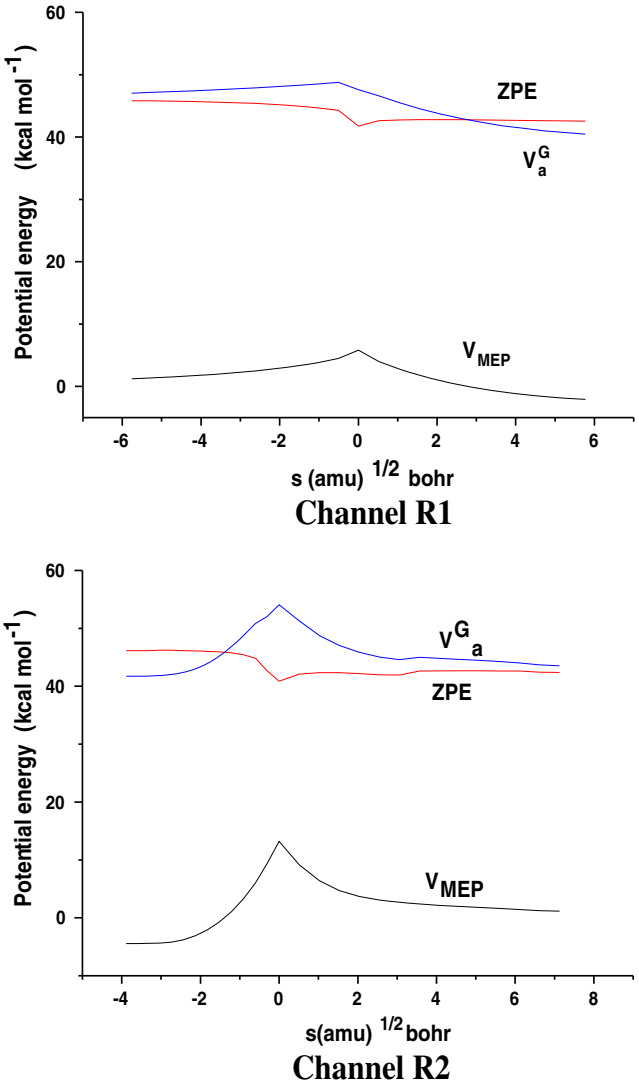

Fig. 3 Classical potential energy curve (V_{MEP}), ground state vibrationally adiabatic energy curve (V_a^G), and zero-point energy curve (ZPE) as functions of s (in $(amu)^{1/2}$ bohr) at the CCSD(T)//BHandHLYP/6-311G** level for reaction channels R1 and R2

Rate coefficient calculations

Dual-level direct dynamics calculations are carried out to evaluate the rate coefficients of the title reaction. The minimum energy path (MEP) is calculated by intrinsic reaction coordinate (IRC) theory at the BHandHLYP/6-311G** level of theory and the potential energy surface (PES) information is further improved with the CCSD(T) level of theory. In the recent work [15], the rate coefficients of each possible reaction pathway were calculated through the transition state theory (TST) using Wigner's transmission coefficient to include the tunneling effect corrections. The Wigner correction they used seems not effective because the theoretical results will be accurate enough only when the tunneling effect is determined by the potential energy surface properties near the saddle point. The comparison of their computational and experimental results shows obvious deviation from each other. Theoretically calculated rate coefficients (in units of cm^3 $molecule^{-1}$ s^{-1}) at different temperatures through TST are in the numerical level of 10^{-12} or 10^{-11} which are much larger than the experimental counterparts (10^{-13} in units of cm^3 $molecule^{-1}$ s^{-1}). In

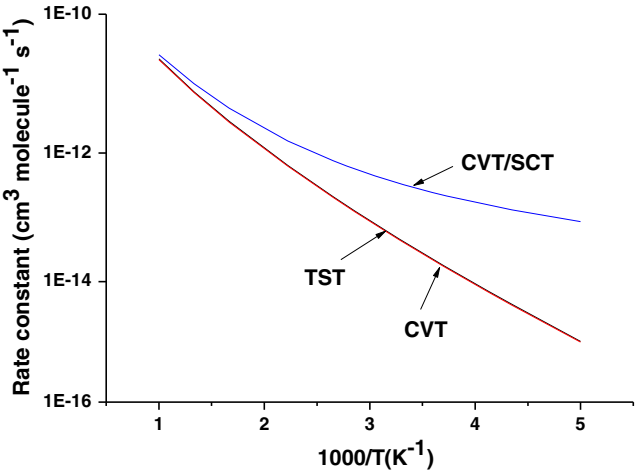

Fig. 4 Computed TST, CVT, and CVT/SCT rate constants as a function of 10^3/T for the reaction channel R1

the present work, the rate coefficients are calculated by the conventional transition-state theory (TST), the canonical variational transition-state theory (CVT), and CVT coupled with the small-curvature tunneling (SCT) correction in the temperature range of 200–600 K. The plots of the TST, CVT, and CVT/SCT rate coefficients for the reaction channels R1 are shown in Fig. 4. It could be found from this figure that the TST and CVT curves are almost the same, implying that the variational effect is small for the reaction channel R1. The phenomena are consistent with previous MEP analysis. It could also be seen from these figures that the curves of CVT and CVT/SCT are drawing near at high temperatures and both the curves become separate gradually with the decrease of temperature. That is to say, the tunneling effect plays a significant role in the lower temperature region for the title reaction. The results are quite noticeable in these figures, which tally with the character of the hydrogen transfer reaction. Table 3 lists the calculated rate coefficients (in $cm^3molecule^{-1}s^{-1}$) as well as experimental results for the title reaction, where k_1, k_2, and k stand for the CVT/SCT rate coefficients for the channel R1, channel R2, and total rate coefficients, respectively. It could be found that channel R1 contributes the most part to the total rate coefficients whereas channel R2 plays a minor role and could be ignored. Thus, we could reach the conclusion that the total rate coefficients of the title reaction are nearly equal to the rate coefficients of the reaction channel R1. It could also be seen that the rate coefficients increase rapidly with elevation of temperature. For example, the CVT/SCT rate coefficient of the reaction is $8.94\times10^{-14}cm^3$ $molecule^{-1}s^{-1}$ at 200 K and the CVT/SCT rate coefficient of the reaction is $4.60\times10^{-12}cm^3molecule^{-1}s^{-1}$ at 600 K. Thus, the reaction should play an important role under high-temperature conditions. The comparison of the calculated total rate coefficients and the experimental values for the title reaction is plotted in Fig. 5. It could be found that the calculated rate coefficients are in good agreement with all the available experimental values [15]. What is more, our calculated results are much better than the recently calculated results [15]. This is largely due to the better method adopted for calculating the potential energy surface of the title reaction and the transition state theoretical method used for calculating the rate coefficients. For the convenience of future experimental measurements, the four parameter fit for the total rate coefficients [36] of the title reaction within 200–1000 K is made and the expression is as follows (in units of $cm^3molecule^{-1}s^{-1}$):

$$k = 3.3\times10^{-11}\left(\frac{T-95.83}{300}\right)^{1.43}\exp\left[\frac{-16485\times(T-95.83)}{R\times\left(T^2+9183.4\right)}\right]$$

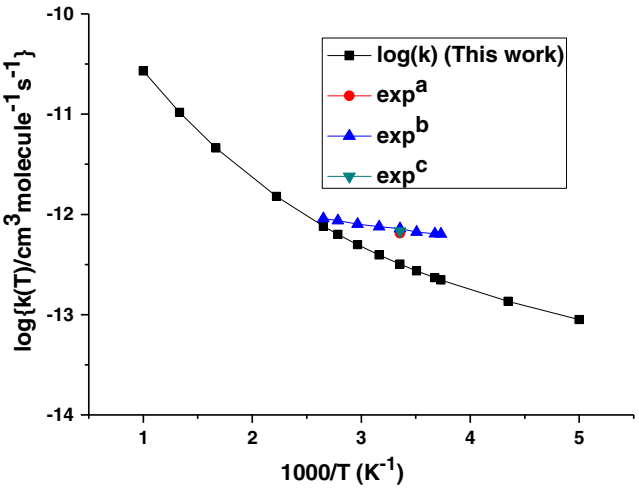

Fig. 5 Calculated Arrhenius plots of the rate constants at the CCSD(T)//BHandHLYP/6-311G** level of theory of the reaction versus 1000/T(K^{-1}) and the available experimental values: [a] The experimental values from ref 11. [b] The experimental values from ref 15. [c] The experimental values from refs 14

Conclusions

The theoretical investigation of the reaction mechanism and kinetics of 2,2,3,3,3-pentafluoropropanol ($CF_3CF_2CH_2OH$) reaction with chlorine atom (Cl) is performed in this study. Two hydrogen abstraction channels of the title reaction are identified. The geometries of the stationary points in the potential energy surface are obtained at the BHandHLYP/6-311G** level, and the energies of the selected points along the minimum energy path (MEP) are further improved by the CCSD(T) method. There exist the complexes with energies lower than the corresponding reactants or products for each hydrogen abstraction channel. A dual-level direct dynamics method is employed to study the kinetic nature of the hydrogen-abstraction reaction. The calculated rate coefficients show that the hydrogen abstraction from the CH_2 group is the primary channel and the contribution of the other channel through hydrogen abstraction from OH group in the reactant $CF_3CF_2CH_2OH$ plays the minor role and could be ignored. The variational effect is small over the whole temperature range for the reaction channels R1 and R2, and the tunneling effect plays a significant role at low temperatures. The calculated total rate coefficients using the canonical variational transition-state theory (CVT) with small-curvature tunneling (SCT) correction are in best agreement with the experimental values. The four-parameter rate coefficients expression of the title reaction between the temperatures 200 K and 1000 K is also provided.

Acknowledgments This work is supported by the Natural Science Foundation of China (Grant No.20973076 and 21173096) and Specialized Research Fund for the Doctoral Program of Higher Education (20110061110018). Thanks are due to the reviewers for many valuable comments.

References

1. Ravishankara AR, Turnipseed AA, Jensen NR, Barone S, Mills M, Howard CJ, Solomon S (1994) Science 263:71–75
2. WMO/UNEP, 2010: Scientific Assessment of Ozone Depletion
3. Furon T (1990) Manyuaru S. Fluorocarbon Manufacturers Association, Tokyo, Japan
4. Singh HB, Kasting JF (1988) J Atmos Chem 7:261–285
5. Spicer W, Chapman EG, Finlayson-Pitts BJ, Plastridge RA, Hubbe JM, Fast JD, Berkowitz CM (1998) Nature 394:353–356
6. Finlayson-Pitts BJ, Pitts JN (2000) Chemistry of the upper and lower atmosphere. Academic, New York
7. Tanaka PL, Riemer DD, Chang SH, Yarwood G, McDonald-Buller EC, Apel EC, Orlando JJ, Silva PJ, Jimenez JL, Canagaratna MR, Neece JD, Mullins CD, Allen DT (2003) Atmos Environ 37:1393–1400
8. Tanaka PL, Oldfield S, Neece JD, Mullins CB, Allen DT (2000) Environ Sci Technol 34:4470–4473
9. Tokuhashi K, Nagai H, Takahashi A, Kaise M, Kondo S, Sekiya A, Takahashi M, Gotoh Y, Suga A (1999) J Phys Chem A 103:2664–2672
10. Chen L, Fukuda K, Takenaka N, Bandow H, Maeda Y (2000) Int J Chem Kinet 32:73–78
11. Hurley MD, Wallington TJ, Sulbaek MP, Andersen S, Ellis DA, Martin JW, Mabury SA (2004) J Phys Chem A 108:1973–1979
12. Antinolo M, Gonzalez S, Ballesteros B, Albaladejo J, Jimenez E (2012) J Phys Chem A 116:6041–6050
13. Wang Y, Liu J, Li Z, Wang L, Wu J, Sun C (2006) J Phys Chem A 110:5853–5859
14. Papadimitriou VC, Papanastasiou DK, Stefanopoulos VG, Zaras AM, Lazarou YG, Papagiannakopoulos P (2007) J Phys Chem A 111:11608–11617
15. Garzon A, Antinolo M, Moral M, Notario A, Jimenez E, Fernandez-Gomez M, Albaladejo J (2013) Mol Phys 111:753–763
16. Becke AD (1993) J Chem Phys 98:1372–1377
17. Lee C, Yang W, Parr RG (1988) Phys Rev B 37:785–789
18. Yang L, Liu JY, Li ZS (2008) J Phys Chem A 112:6364–6372
19. Yu AY, Zhang HX (2013) Mol Phys doi:10.1007/s00894-013-1960-3
20. Scuseria GE, Schaefer HF (1989) J Chem Phys 90:3700–3703
21. Pople JA, Gordon MH, Raghavachari K (1989) J Chem Phys 87:5968–5975
22. Frisch MJ, Trucks GW, Schlegel HB et al. (2009) Gaussian 09. Revision X. Gaussian Inc, Wallingford, CT
23. Truhlar DG (1995) In: Heidrich D (Ed.) The reaction path in chemistry: current approaches and perspectives; Kluwer, Dordrecht, the Netherlands, p 229
24. Fernandez-Ramos A, Miller JA, Klippenstein SJ, Truhlar DG (2006) Chem Rev 106:4518–4584
25. Hu WP, Truhlar DG (1995) J Am Chem Soc 117:10726–10734
26. Garrett BC, Truhlar DG (1979) J Chem Phys 70:1593–1598
27. Liu YP, Lynch GC, Truong TN, Liu DH, Truhlar DG, Garrett BC (1993) J Am Chem Soc 115:2408–2415
28. Steckler R, Hu WP, Liu YP, Lynch GC, Garrett BC, Isaacson AD, Melissas VS, Lu DP, Troung TN, Rai SN, Hancock GC, Lauderdate JG (1995) Comput Phys Commun 88:341–343
29. Truhlar DG (1991) J Comp Chem 12:266–270
30. Chuang YY, Truhlar DG (2000) J Chem Phys 112:1221–1228
31. Liu YP, Gonzàlez-Lafont A, Truhlar DG, Garrett BC (1993) J Am Chem Soc 115:7806–7817
32. Truhlar DG, Isaacson AD, Garrett BC (1985) In Theory of Chemical Reaction Dynamics; Baer, M., Ed.; 4: 65-137
33. Truhlar DG, Isaacson AD, Skodje RT, Garrett BC (1982) J Phys Chem 86:2252–2261
34. Chang YY, Corchado JC, Fast PL, Villa J, Hu WP, Liu YP, Lynch GC, Jackels CF, Nguyen KA, Gu MZ, Rossi I, Coitino EL, Claylon S, Melissas VS, Lynch BJ, Steckler R, Garrett BC, Isaacson AD, Truhlar DG (2007) POLYRATE version 9.6. University of Minnesota, Minneapolis
35. Scheiner S, Seybold PG (2009) Struc Chem 20:43–48
36. Zheng J, Truhlar DG (2012) Faraday Discuss 157:59–88